Polypropylene Nanocomposites Prepared with Natural and ODTABr-Modified Montmorillonite

Sevim İşçi,[1] Cüneyt H. Ünlü,[2] Oya Atıcı[2]

[1]*Department of Physics, Istanbul Technical University, Maslak, Istanbul 34469, Turkey*
[2]*Department of Chemistry, Istanbul Technical University, Maslak, Istanbul 34469, Turkey*

Received 7 September 2008; accepted 4 December 2008
DOI 10.1002/app.29853
Published online 19 March 2009 in Wiley InterScience (www.interscience.wiley.com).

ABSTRACT: In this study, the main goal is to obtain montmorillonite nanocomposites of polypropylene (PP). To achieve this goal, a two-phase study was performed. In the first part of the work, organomodified clay (OMMT) was synthesized and characterized. Octadecyltrimethylammonium bromide (ODTABr) cationic surfactant was added to the clay (Na-activated montmorillonite, MMT) dispersions in different concentrations in the range of 5×10^{-5}–1×10^{-2} mol/L. Rheologic, electrokinetic, and spectral analyses indicated that ODTABr has interacted with MMT at optimum conditions when the concentration was 1×10^{-2} mol/L. In the second part, modified (OMMT) and unmodified (MMT) montmorillonite were used to obtain PP nanocomposites (OMMT/PP and MMT/PP, respectively). The nanocomposites were prepared by melt intercalation where the montmorillonite contents were 1 or 5% (w/w) for each case. The thermal analyses showed that the thermal properties of OMMT/PP nanocomposites were better than MMT/PP, and both of them were also better than pure polymer. Increase in the concentration of MMT (or OMMT) decreased the thermal resistance. Based on the IR absorption intensity changes of regularity and conformational bands, it is found that the content of the helical structure of macromolecular chains has increased with increasing concentrations of both MMT and OMMT in the nanocomposites. © 2009 Wiley Periodicals, Inc. J Appl Polym Sci 113: 367–374, 2009

Key words: montmorillonite; organoclay; nanocomposite; helical content; spectral characterization; thermal characterization

INTRODUCTION

Polymer/clay nanocomposites are a typical example of nanotechnology. Layered clay mineral is one of the most interesting layered hosts because of its unique layered structure, cation exchangeability, and expandability. Montmorillonite is the most widely used layered clay mineral in polymer/clay nanocomposite.[1,2] The interlayer spacing of montmorillonite can be expandable by changing the hydrophilic cations residing in the basal spacing with other inorganic or organic cations (generally long-chain alkylammonium cation or phosphonium salt).[1,3] The aim of this kind of modification is to enhance the interaction between the polymeric matrix and clay particles by expanding and changing the polarity of the clay layers. Then, these modified clays can be easily dispersed in polymeric matrix and may form a nanocomposite. When pure polymer and clay nanocomposites are compared, the advantageous properties of polymer/clay nanocomposites are increased modulus and mechanical strength, higher heat distortion temperature, decreased thermal expansion coefficient, lower gas permeability, and superior solvent resistance.[4–11]

Polypropylene (PP) is one of the most widely used polyolefin polymers. It is one of the most interesting thermoplastic materials because of its low price and balanced properties. PP, however, has its defect. Low strength and stiffness, low service temperature, and weak barrier properties do not make PP the most ideal thermoplastic to use. To overcome these problems, traditional filler materials, such as talc and mica, have been infused into the PP structure. Although the fillers increased the strength and stiffness, it reduced the impact properties and recyclability. The uses of layered silicate materials, the macromolecule chains, exfoliate the silicate layers evenly dispersing them in the polymer matrix. For this reason, the utilization of PP is very high. When filled organoclay is used, there are improvements in the mechanical performance,[12–14] thermal stability,[15–17] barrier properties, and flame retardancy[13,18] of the polymer without sacrificing processability and density.

In this study, first, the interactions between MMT particles and octadecyltrimethylammonium bromide (ODTABr) surfactant were determined by using

Correspondence to: O. Atıcı (atici@itu.edu.tr).
Contract grant sponsor: Istanbul Technical University, Research Fund; contract grant number: 30451.

rheologic and electrokinetic parameters. Then, the structural properties of the MMT and OMMT were examined by XRD and FTIR analyses. Second part of the study was related with PP/clay nanocomposites. Nanocomposites were prepared with melt intercalation method. Both types of montmorillonite (MMT and OMMT) were used in different amounts (1 and 5% by weight) to prepare the nanocomposites. Then, PP composites were characterized in terms of their spectral (XRD, FTIR) and thermal behaviors.

EXPERIMENTAL

Materials

The clay sample was obtained from the bentonite deposits in Enez, Turkey (Bensan Co.). The chemical composition of the sample was determined by atomic adsorption spectroscopy, and silica analysis was done by the gravimetric method. The Ca-montmorillonite (natural bentonite) has a composition (wt %) of Al_2O_3 19.00, SiO_2 58.80, Fe_2O_3 3.50, CaO 4.60, MgO 2.80, Na_2O 1.00, K_2O 2.76, TiO_2 0.45, MnO 0.11, and H_2O 7.39. Cationic surfactant, ODTABr [$C_{18}H_{35}N^+(CH_3)_3Br^-$] from Fluka Chemical Co., and isotactic PP (M_W = 12 000) from Aldrich Chemical Co. were used.

Preparation of Na-activated montmorillonite

Activated montmorillonite was obtained from natural montmorillonite (35% humidity) by treating the clay with 4% (w/v) $NaHCO_3$ solution. During soda activation, certain amount of Ca ions was precipitated in the form of $CaCO_3$. Na-activated montmorillonite was labeled as MMT. The chemical composition of this sample was (wt %) as follows: SiO_2 58.8, Al_2O_3 18.73, Fe_2O_3 3.71, CaO 3.34, MnO 0.09, Na_2O 3.36, MgO 2.62, K_2O 2.70, and TiO_2 0.49.

Preparation of OMMT

The minimum ODTABr surfactant concentration, which coagulation occurred in the dispersion, was recorded as the critical coagulation concentration (C_K). For this purpose, dilute (0.25% w/w) bentonite dispersions prepared with different surfactant concentrations, and the C_K was determined by visual inspection at room temperature. The critical coagulation concentration value of MMT was found as 5×10^{-4} mol/L. Hence, ODTABr was added to the MMT dispersions (2% w/w) in the range of 10^{-6}–10^{-2} mol/L for rheologic and electrokinetic characterization.

According to the XRD measurements, the maximum expansion in interlayer spacing was obtained with the 1×10^{-2} mol/L ODTABr concentration. This concentration was adopted to prepare the organoclay by the following method.

Four grams of clay was dispersed in 100 mL of water for 24 h. Then, 100 mL of 0.5*M* ODTABr and catalytic amount of concentrated HCl were added to the dispersion and they were stirred at 80°C for 1 h. After the dispersion was centrifuged, the clay was washed with water at 80°C two times. Then, the obtained organoclay was dried at 40°C.

Preparation of PP nanocomposites

PP was melted at 190°C. Then, the composites were prepared using the clay samples (OMMT and MMT, respectively) as reinforcement for PP in both cases. The clay was added to molten PP at the solid concentration of 1 and 5% (w/w). Then, the samples were dried at the room conditions.

Characterization of MMT, OMMT, MMT/PP, and OMMT/PP

X-ray diffraction (Philips PW1140 model XRD) and FTIR (Perkin–Elmer Spectrum One spectrophotometer) techniques were used to determine the clay mineral types. The dominant clay mineral was found to be dioctahedral montmorillonite with minor amounts of illite and kaolinite. Quartz was always present in the clay fraction. The *d*-spacing of the MMT, OMMT, MMT/PP, and OMMT/PP compounds are calculated using Bragg's equation according to the angle of the (001) diffraction peaks in the XRD pattern. Crystal structure and dimensions of PP were determined via 110, 040, and 130 plane peaks.[19–21]

The zeta potential measurements were carried out using a Malvern Instruments, Zetasizer 2000. The optic unit contains a 5 mW He–Ne (638 nm) laser. Before the measurements, all the dispersions were centrifuged at 4500 rpm for 30 min. Supernatants were then used for zeta potential measurements.

The flow behavior of the dispersions was measured in a Brookfield DVIII + type low-shear rheometer. The sample was dispersed in water (2%, w/w) and shaken overnight. An adsorption time of 24 h was adopted for the surfactant. The rheologic behavior of the clay suspensions was obtained by shear stress-shear rate measurements within 0–350 s^{-1} shear rates. Rheologic measurements were carried out in duplicate.

FTIR analyses (400–4000 cm^{-1}) were performed on 1% (w/w) concentration KBr pellets. All spectra were obtained in the wavenumber range of 4000–400 cm^{-1}. Spectral outputs were recorded either in the absorbance or transmittance mode. In FTIR spectra, the peaks at wavenumber of 841, 973, 998, and 1220 cm^{-1} were assigned to form helical conformation.

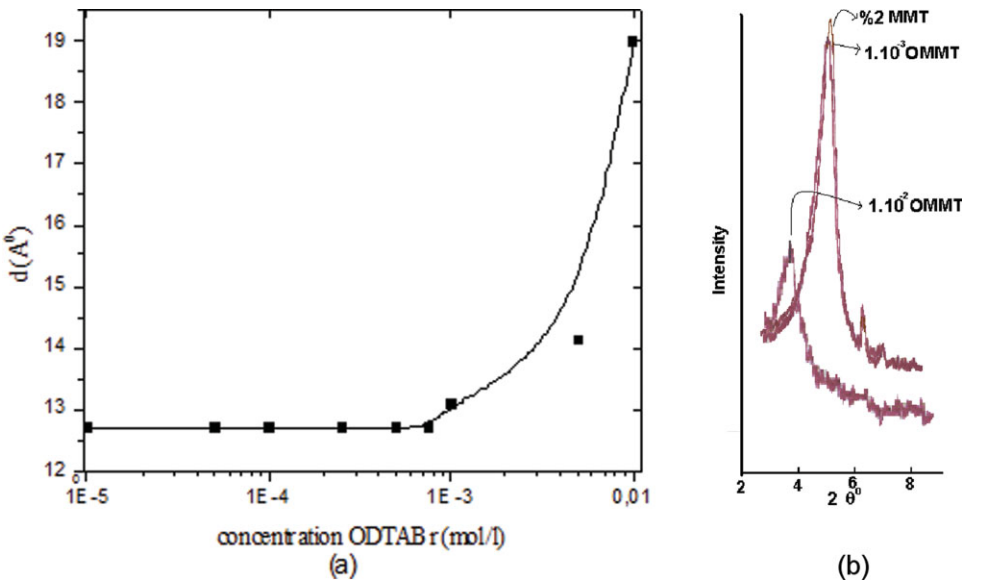

Figure 1 (a) Variations in basal spacing (d_{001}) in Å as a function of surfactant concentrations in the bentonite suspension. (b) XRD patterns of MMT, 1×10^{-3} mol/L OMMT, and 1×10^{-2} mol/L OMMT. [Color figure can be viewed in the online issue, which is available at www.interscience.wiley.com.]

The minimum numbers of repeating units, (n), in the helical sequences were determined as 5, 10, 12, and 14, respectively.[11] Apparently, the larger the value of n, the higher the degree of order of the corresponding regularity bands. The ratio of the absorbance ratio of regularity bands at 998 to 973 cm^{-1} was taken as the percentage of helical content. This ratio has been related to the percentage of isotactic polymer.

Thermogravimetric analysis (TGA) was carried out in the temperature range of 30–600°C at a heating rate of 20°C/min under a nitrogen atmosphere on a TGA Q50.

Differential scanning calorimetry (DSC) was performed in a Perkin–Elmer Diamond at a heating rate of 20°C/min under a nitrogen atmosphere and in the temperature between 10 and 280°C.

RESULTS

Microstructure, electrokinetic, and flow properties of MMT and OMMT dispersions

XRD measurements, electrokinetic and rheologic parameters, were used to characterize the clay-surfactant dispersions.

The basal space of MMT layers was determined as a function of ODTABr concentration [Fig. 1(a)]. It was found that ODTABr showed the intercalation and expansion effect of the interlayer of MMT. Figure 1(b) shows the XRD patterns of MMT and MMT with ODTABr at the concentration of 10^{-3} and 10^{-2} mol/L. The basal spacing value of MMT, 10^{-3} mol/L ODTABr-MMT, and 10^{-2} mol/L ODTABr-MMT was found to be 12.71, 13.08, and 18.98 Å, respectively. XRD results indicated a bilayer- or pseudotrilayer-type arrangement of the ODTABr molecules parallel to the silicate layer.[18,22–25] The XRD measurements showed that the d_{001} has been extended to the biggest value at the concentration of 10^{-2} mol/L surfactant to the 2% MMT dispersions. Hence, this concentration was chosen to prepare organoclay samples. The interlayer distance of the clay particles was also expanded by the method and d_{001} value was expanded to 21.8 Å.

The zeta potential value was −41.8 mV for the MMT dispersions. This value displays deflocculating structure of dispersion. In Figure 2, the zeta potential of MMT dispersions was plotted as a function of

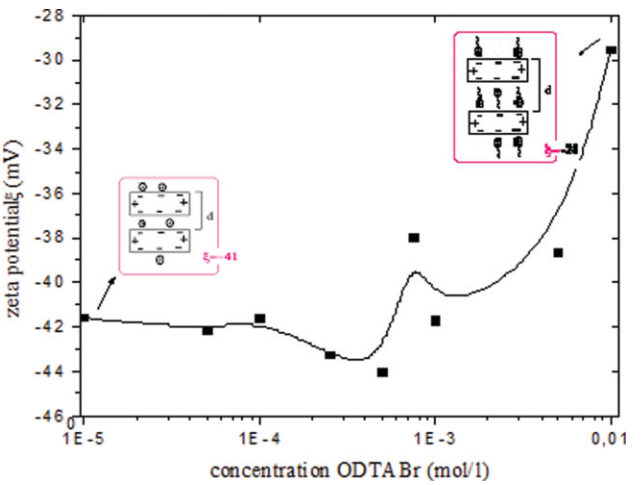

Figure 2 The zeta potential of the MMT sample as a function of surfactant concentration. [Color figure can be viewed in the online issue, which is available at www.interscience.wiley.com.]

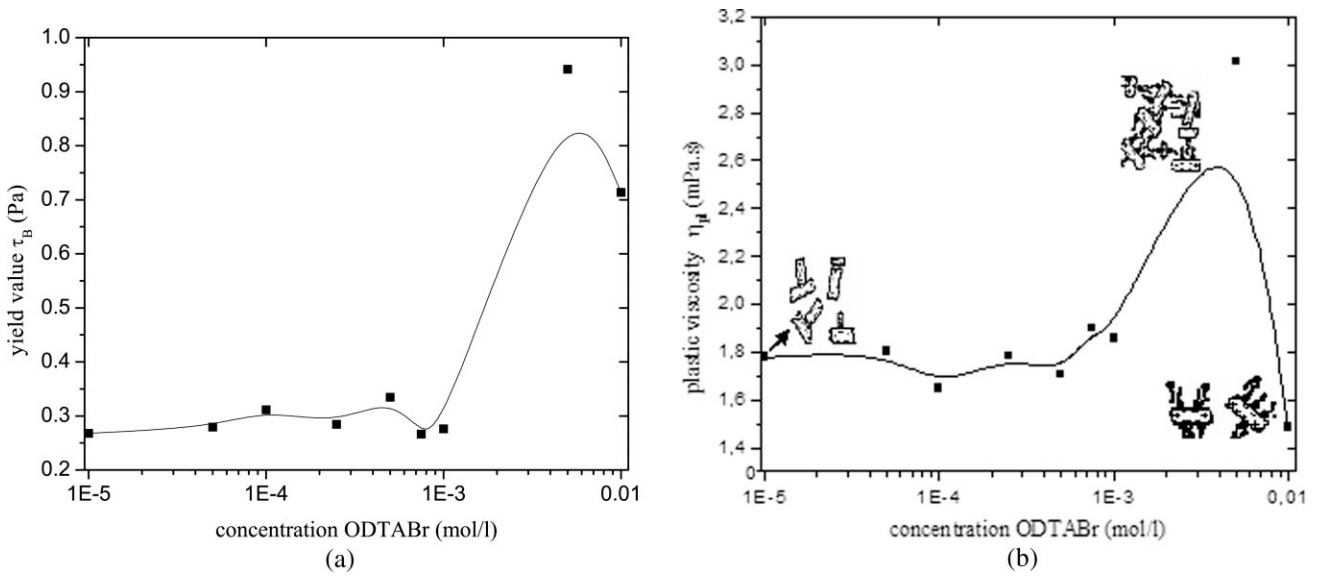

Figure 3 The changes of (a) the yield value, (b) plastic viscosity of MMT dispersions with ODTABr surfactant added to dispersions.

increasing surfactant concentration. The absolute value of zeta potential decreased with the increasing surfactant concentration. This decrease was observed clearer at higher concentrations of ODTABr. The ODTABr surfactant showed flocculant effect on the MMT. The dispersion became more flocculated after the addition of ODTABr and began to aggregate by adsorbing cationic ODTABr on the negatively charged MMT. However, ODTABr was not able to cover up completely clay surfaces even at the highest concentration.

The MMT dispersion showed Bingham plastic flow properties and the flow behavior of the montmorillonite dispersions did not change by the addition of ODTABr. In Figure 3(a,b), the yield value (τ_B) and plastic viscosity (η_{Pl}) of MMT dispersions were plotted as a function of ODTABr concentration. It was observed that the effect of the surfactant was similar on both τ_B and η_{Pl}. The yield stress and plastic viscosity reached the maximum values at 5×10^{-3} mol/L surfactant concentration. At the lower concentrations, the dispersions were more or less stable, but flocculation started around that the maximum value and then particles started to settle down.

The structural characterization of MMT and OMMT was also determined with FTIR

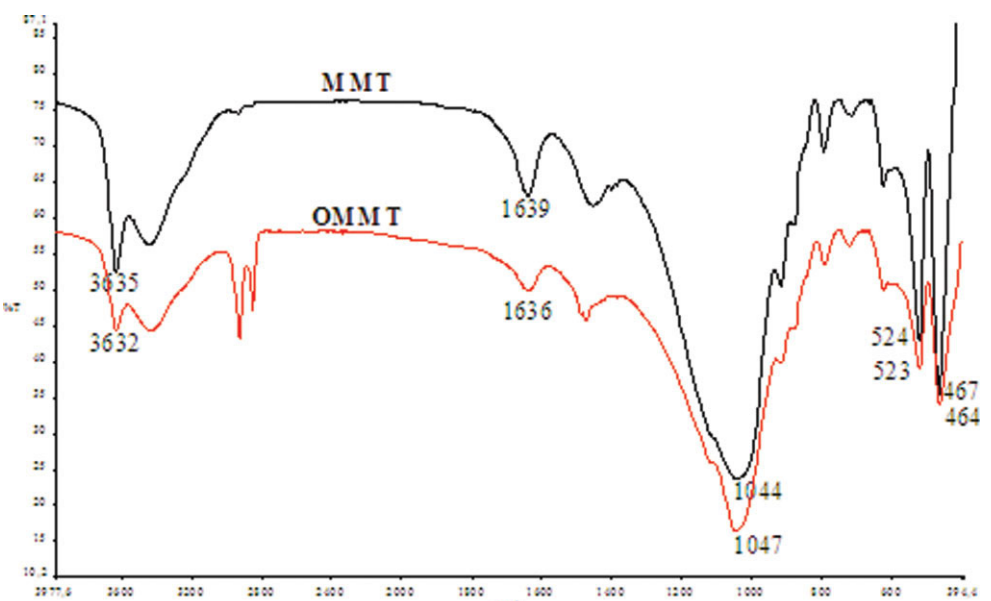

Figure 4 FTIR spectra of unmodified and 1×10^{-2} mol/L ODTABr-modified montmorillonite. [Color figure can be viewed in the online issue, which is available at www.interscience.wiley.com.]

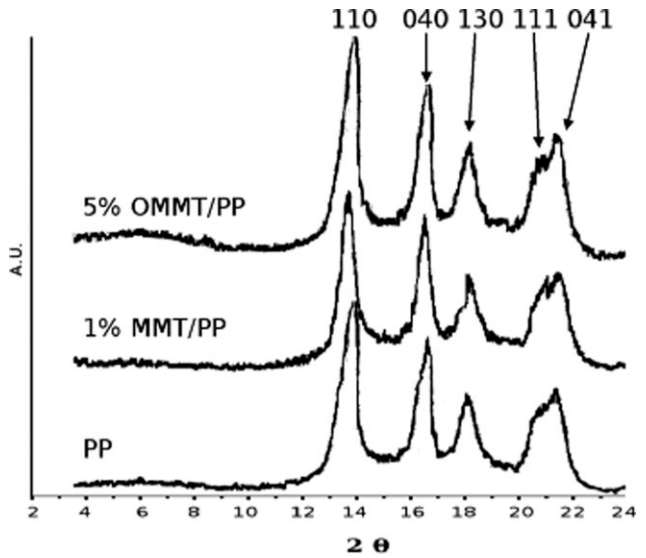

Figure 5 XRD patterns of PP, 1% MMT/PP, and 5% OMMT/PP samples.

measurements (Fig. 4). The spectrum of MMT showed the characteristic bands at 3635 cm^{-1} because of structural O—H and intralayer and interlayer H-bonded O—H stretching as a broad peak centered at 3442 cm^{-1}, H—O—H bending at 1639 cm^{-1}, Si—O stretching at 1044 cm^{-1} with shoulder at 1114 cm^{-1}, OH deformation linked to cation at 919, 882, 795, and 625 cm^{-1}, and Si—O bending at 524 and 467 cm^{-1}. Bands at 1454, 877, and 713 cm^{-1} were evidence of the presence of calcite.[26] The exchange of simple inorganic cations with the surfactants resulted in the enhancement of the band intensities of the 3500–3200 cm^{-1} band, along with a reduction of intensities because of Si—O and Al—O stretching. The increase in the intensities of the peaks at 3500–3200 cm^{-1} reflected the increased hydrogen bonding between the lattice hydroxyls and organic groups of MMT. When the protons of ODTABr made hydrogen bonds with the oxygen species of Si—O, Al—O, and Si—O—Al segment, Si—O, Al—O, and Si—O—Al bonds weakened resulting in distortion of the tetrahedral symmetry of these moieties. This is resulted in the change of the IR band positions as well in their intensities. It could clearly be seen that the OMMT spectra exhibited the presence of characteristic absorptions of the organic and inorganic groups (Fig. 4). Absorbencies because of structural O—H stretching at 3632 cm^{-1}, OH deformation linked to cation (Mg, Al—OH, Al—O), and Si—O bending at 920, 884, 794, 626, 523, and 464 cm^{-1} confirmed the presence of MMT in the dispersion. On the other hand, absorptions at 2926 and 2852 cm^{-1} (aliphatic C—H asymmetrical and symmetrical stretching), 1484, 1473, and 1385 cm^{-1} (aliphatic C—H bending), and characteristic asymmetrical C—H bending of ammonium cation at 1489 cm^{-1} were the evidences for the presence of the ODTABr. As ODTABr adsorbed on MMT, the O—H stretching peak was broadened giving a maximum at 3421 cm^{-1}. The hydroxyl stretching frequencies were also broadened and bands have drifted to lower frequencies by about 20 cm^{-1}. These shifts may be attributed to the formation of hydrogen bonds.[27] These hydrogen bonds of ODTABr also resulted in the weakening of H—O—H bending vibration band, which can be explained by the replacement of metal ions by ODTABr via ion exchange. The Si—O stretching peak was broadened and gave a maximum at 1047 cm^{-1} with shoulder at 1116 cm^{-1}. This was attributed to the relaxation of hydrogen bonding between Mg, Al—OH, as well as to the hydrated water of exchangeable cationic metal ions on the montmorillonite surface, further supporting the presence of ODTABr. On the other hand, adsorption bands of Al—O vibration for ODTABr containing MMT sample were also different than those for MMT. This was attributed to the relaxation of hydrogen bonding between (Al—O)O—H deformations as well as to the hydrated water of exchangeable cationic metal ions on the montmorillonite surface. This observation was in agreement with our explanation of the change in zeta potential and XRD studies.

Characterization of MMT/PP and OMMT/PP nanocomposites

XRD patterns of pure PP, MMT/PP, and OMMT/PP nanocomposites are shown in Figure 5. As indicated in the figure, (d_{001}) basal spacing peaks of MMT and OMMT could not be observed for 1% MMT/PP and for 1 and 5% OMMT/PP nanocomposites. This occasion may be attributed to the surrounding of montmorillonite by polymer chains. However, crystalline structure of PP has changed relying on XRD pattern. Diffraction peaks of PP and nanocomposites are listed in Table I. These diffraction planes were related with the crystal structure of PP. The diffraction planes of monoclinic structure of PP are 110, 040, and 130. Diffraction peaks of pure PP and nanocomposites did not show much difference, indicating

TABLE I
Diffraction Peaks of Pure PP and OMMT/PP, MMT/PP Nanocomposites

Material	Diffraction planes (2θ)				
	110	040	130	111	041
PP	14.4	17.0	18.5	21.1	21.7
1% MMT/PP	13.7	16.5	18.1	21.0	21.4
5% MMT/PP	14.2	17.0	18.6	21.3	21.7
1% OMMT/PP	14.1	16.9	18.4	21.1	21.7
5% OMMT/PP	14.1	16.9	18.5	21.1	21.7

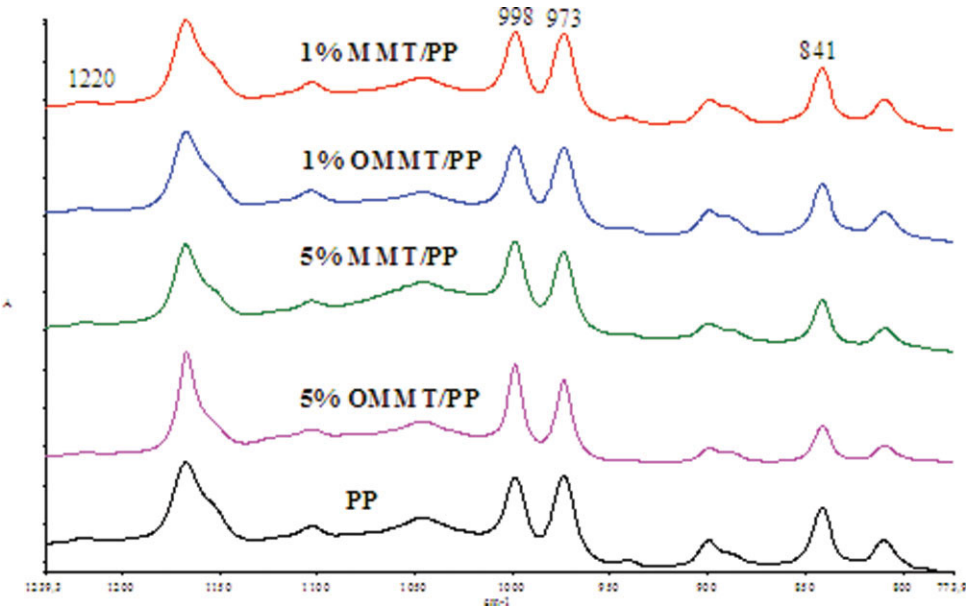

Figure 6 Regularity bands of polypropylene composites samples from modified and unmodified montmorillonite. [Color figure can be viewed in the online issue, which is available at www.interscience.wiley.com.]

retention of monoclinic structure. Very small changes in peak maxima showed that the crystallite dimensions were remained nearly unchanged.

FTIR spectra of the nanocomposites exhibited the presence of characteristic absorptions of both organic and inorganic groups. The montmorillonite peaks were appeared by the OH stretching at 3410–3432 cm^{-1}, adsorbed HOH bending at 1643–1647 cm^{-1}, Si—O stretch at 1045–46 cm^{-1}, and Si—O bending at 518–26 and 457–61 cm^{-1}. The absence of a structural —OH stretch at 3632 cm^{-1} in pure PP confirmed the purity of the product. Absorptions, on the other hand, at 2960, 2922, 2870, and 2839 cm^{-1} (asymmetric and symmetric C—H stretching vibration), 1461 cm^{-1} (asymmetric C—H deformation), 1378 cm^{-1} (symmetric C—H deformation), 1167 cm^{-1} (backbone C—C stretching), 998 cm^{-1} (CH_3 rocking, crystalline region for isotactic PP), 973 (CH_3 rocking, amorphous region for PP), 841 (C—C stretching, CH_2, CH_3 rocking), and 810 cm^{-1} (C—H deformation out-of-plane) were characteristic FTIR absorption bands for isotactic PP. These results indicated that the PP molecules were incorporated into the clay structure. In addition, infrared spectroscopy is a tool, which is widely used to study the conformational properties of polymers. The domain structures of the segmented MMT/PP and OMMT/PP were analyzed by FTIR as shown in Figure 6. For isotactic PP, most of the absorption bands, which appear in the frequency region below 1400 cm^{-1}, are related with the regularity of PP and they are connected with intramolecular vibration coupling in an individual chain.[11,28] The peaks at wavenumbers of 973, 998, 841, and 1220 cm^{-1} were assigned to helical form conformation. The appearance of these regularity bands reflected the existence of helical sequences. A parameter commonly used to measure the overall relative helical-to-planar ratio of isotactic PP is the absorbance ratio A_{998}/A_{973}. Comparison of these peaks gave reliable and reproducible results for helical content amount of PP in nanocomposites.

Relying on the analyses, which their results summarized in Table II, we could say that increasing clay amount (both MMT and OMMT) has resulted in an increase in the helical content of the nanocomposites. It exhibited that the conformational order of the

TABLE II
The Intensity Ratios of Regularity Bands in FTIR Spectra of Pure and Clay-Added PP Samples

		MMT/PP		OMMT/PP	
	PP	1%	5%	1%	5%
$A_{998\ cm^{-1}}/A_{973\ cm^{-1}}$	0.9421	0.9464	0.9512	0.9446	0.9482
$A_{1220\ cm^{-1}}/A_{973\ cm^{-1}}$	0.1618	0.1682	0.2905	0.1678	0.2296
$A_{1220\ cm^{-1}}/A_{998\ cm^{-1}}$	0.1718	0.1777	0.3054	0.1759	0.2422
$A_{841\ cm^{-1}}/A_{973\ cm^{-1}}$	0.9298	0.9496	0.9749	0.9472	0.9656
$A_{841\ cm^{-1}}/A_{998\ cm^{-1}}$	0.9870	1.0034	1.0249	1.0034	1.0190

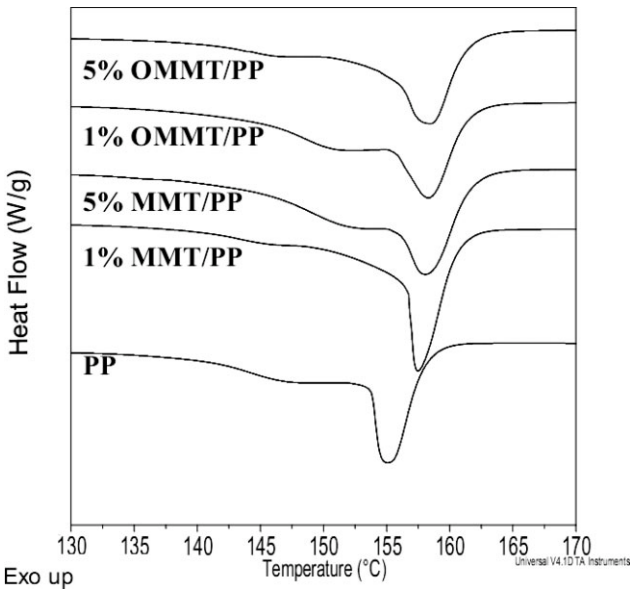

Figure 7 DSC dynamic scan at 20°C/min, for the polypropylene and polypropylene nanocomposites from modified and unmodified montmorillonite

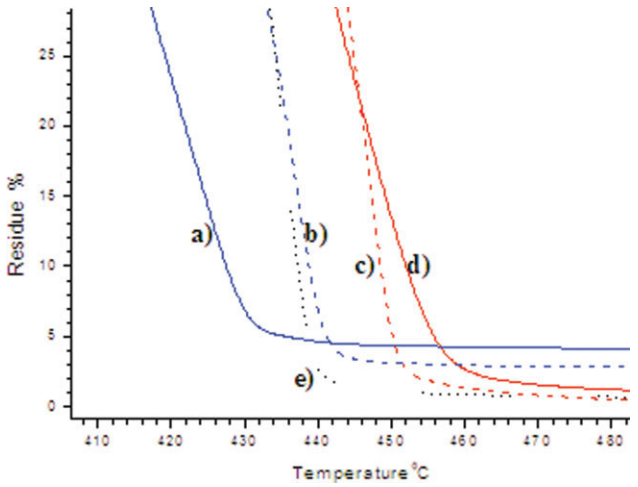

Figure 8 Percent weight loss during a TGA dynamic test at 20°C/min in nitrogen for the (a) 5% MMT/PP, (b) 5% OMMT/PP, (c) 1% MMT/PP, (d) 1% OMMT/PP, and (e) PP. [Color figure can be viewed in the online issue, which is available at www.interscience.wiley.com.]

sample increases with reduction in concentrations of pure PP. In addition, helical content of composites with MMT/PP were found more according to the OMMT/PP composite.

Thermal Characterization of PP, MMT/PP, and OMMT/PP

In Figures 7 and 8, DSC thermograms and TGA curves are plotted as a function of temperature for pure PP and nanocomposites, respectively. Table III summarizes the experimental results. The melting point of pure PP and the nanocomposites was determined with DSC analysis. The melting point was measured as 155°C for PP. As the clay added to PP, higher melting point values were observed (for 1 and 5% clay addition 2 and 3.5°C higher, respectively). The maximum weight loss temperatures were observed as 435°C for PP. This value increased after the clay and organoclay loading of 1%. This implied that clay and organoclay were effective in improving the thermal stability of the PP systems. As seen from the table, the thermal stability of the products increased about 10°C higher temperatures. Nevertheless, increasing concentration of the clay and organoclay caused to decrease on the thermal resistance. The lower concentration of clay particles dispersed in the polymer matrix better than the higher concentration ones. Hence, the well dispersed particles caused to better thermal resistance. Except the 5% of OMMT, all the residues of the nanocomposites showed increased values at maximum weight loss temperatures. All the nanocomposites had more residue than the pure polymer at 450°C.

CONCLUSIONS

In this work, with electrokinetic measurements, it was successfully shown that the surfactant

TABLE III
DSC Melting Data and Thermogravimetric Analysis Results of Pure PP and Nanocomposite Samples with Different Types of Montmorillonite

Material	T_m (°C)	T_D^{maxa} (°C)	W_R^b (%)	T_{60}^c (°C)	W_{400}^d (%)	W_{450}^d (%)
PP	155.06	435.01	20.66	430.93	84.12	1.14
1% MMT/PP	157.47	445.64	25.42	437.85	78.83	13.54
5% MMT/PP	157.96	421.27	21.24	410.28	53.97	4.35
1% OMMT/PP	158.26	444.87	23.30	432.00	84.23	5.44
5% OMMT/PP	158.45	432.36	19.99	425.40	70.12	3.13

[a] Maximum weight reduction temperature.
[b] Weight percent of residue at maximum weight loss temperature.
[c] 60% weight loss temperature.
[d] Weight percent of residue at 400 and 450°C.

molecules attached to the negative charged surface of the clay particles and reduced the electrostatic repulsion between clay particles.

XRD results showed that the surfactant molecules were not able to expand the interlayer of the clay particle until 10^{-3} mol/L surfactant concentration. At the 10^{-2} mol/L concentration of surfactant caused to expand the interlayer of clay to 6.27 Å. Also the preparation procedure increased the expansion of the interlayer spacing of the clay particles.

We prepared polymer/clay (MMT/PP) and polymer/organoclay (OMMT/PP) nanocomposites and characterized them with spectral (XRD and FTIR) and thermal (DSC and TGA) techniques.

We also determined that the organoclay/polymer nanocomposites showed higher thermal resistance comparing to clay/polymer nanocomposites. Increase in the concentration of clay (or organoclay) decreased the thermal resistance. The highest thermal resistance observed for 1% of OMMT/PP nanocomposites.

XRD analyses indicated that montmorillonite particles were surrounded by PP chains. This occasion was deducted from 001 plane diffraction peak of montmorillonite, which was not observed in nanocomposite samples. Also, very small changes in 110, 040, and 130 plane diffraction peaks showed that the distortion of crystal shape and dimensions was remained nearly unchanged. And finally, the ratio of the absorbance at 998 cm^{-1} to the absorbance at 973 cm^{-1} (A_{998}/A_{973}) was taken as the percentage of helical content. This ratio was related to the percentage of isotactic polymer and to the percentage of crystallinity with some adjustment. FTIR results indicated that the PP molecules were incorporated into the clay structure, and the proportion of helical sequences increased with increasing the concentrations both of MMT and OMMT. Therefore, the A_{998}/A_{973} absorbance ratio increased steadily during composite formation and was interpreted as an increase in helical ordering, which resulted from backbone scission.

The authors thank Prof. Dr. Ö. Işık Ece for XRD measurements.

References

1. Pinnavaia, T. J.; Beall, G. W. Polymer-Clay Nanocomposites; Wiley: Chichester, 2000.
2. Ray, S. S.; Okamoto, M. Prog Polym Sci 2003, 28, 1539.
3. Isci, S.; Ece, O. I.; Gungor, N. J Compos Mater 2006, 40, 1105.
4. Chang, J.-H.; An, Y. U. J Polym Sci Part B: Polym Phys 2002, 40, 670.
5. Chang, J.-H.; An, Y. U.; Sur, G. S. J Polym Sci Part B: Polym Phys 2003, 41, 94.
6. Chang, J.-H.; Park, D.-K.; Ihn, K. J. J Polym Sci Part B: Polym Phys 2001, 39, 471.
7. Hu, Y.; Song, L.; Xu, J.; Yang, L.; Chen, Z.; Fan, W. Colloid Polym Sci 2001, 279, 819.
8. Jung-Bae, J.; Suh, K.-D. J Appl Polym Sci 2003, 90, 458.
9. Kim, J.-Y.; Jung, W.-C.; Park, K.-Y.; Suh, K.-D. J Appl Polym Sci 2003, 89, 3130.
10. Zeng, Q. H.; Wang, D. Z.; Yu, A. B.; Lu, G. Q. Nanotechnology 2002, 13, 549.
11. Zhu, X.; Yan, D.; Fang, Y. J Phys Chem B 2001, 105, 12461.
12. Kanny, K.; Moodley, V. J Eng Mater Technol 2007, 129, 105.
13. Morgan, A. B.; Harris, J. D. Polymer 2003, 44, 2313.
14. García-López, D.; Picazo, O.; Merino, J. C.; Pastor, J. M. Eur Polym J 2003, 39, 945.
15. Rong, M. Z.; Zhang, M. Q.; Zheng, Y. X.; Zeng, H. M.; Walter, R.; Friedrich, K. Polymer 2001, 42, 167.
16. Filho, F. G. R.; Jeferson, T. A.; Mélo, M.; Rabello, S.; Silva, S. M. L. Polym Degrad Stab 2005, 89, 383.
17. Krump, H.; Luyt, A. S.; Hudec, I. Mater Lett 2006, 60, 2887.
18. Lagaly, G.; Weiss, A. In Proceedings of the International Clay Conference, Tokyo, 1969, p 61.
19. Xu, W.; Liang, G.; Zhai, H.; Tang, S.; Hang, G.; Pan, W.-P. Eur Polym J 2003, 39, 1467.
20. Kawai, T.; Iijima, R.; Yamamoto, Y.; Kimura, T. Polymer 2002, 43, 7301.
21. Lotz, B. J Macromol Sci B 2002, 41, 685.
22. Jaynes, W. F.; Boyd, S. A. Soil Sci Soc Am J 1991, 55, 43.
23. Lagaly, G. In Layer Charge Characteristics of 2 : 1 Silicate Clay Minerals; Mermut, A. R., Ed.; The Clay Minerals Society: Boulder, CO, 1994.
24. Weiss, A. Clays Clay Miner 1963, 10, 191.
25. Laird, D. A.; Scott, A. D.; Fenton, T. E. Clays Clay Miner 1989, 37, 41.
26. Marel, H. W. v. d.; Beutelspacher, H. Atlas of Infrared Spectroscopy of Clay Minerals and their Admixtures; Elsevier Scientific Publishing: Amsterdam, 1976.
27. Gunister, E.; Unlu, C. H.; Atici, O.; Ece, O. I.; Gungor, N. J Compos Mater 2007, 41, 153.
28. Chen, L.; Zhu, X.; Yan, D. Polym Prepr 2003, 44, 1187.